Martian Water Vapor: Mars Express PFS/LW Observations

Thierry Fouchet, Emmanuel Lellouch, Nikolay I. Ignatiev, François Forget, Dmitry V. Titov, Martin Tschimmel, Franck Montmessin, Vittorio Formisano, Marco Giuranna, M. Maturilli, et al.

Martian water vapor : Mars Express PFS/LW observations .T Fouchet[1,2], E. Lellouch[1], N.I. Ignatiev[3,4], F. Forget[5], D.V. Titov[3,4], M. Tschimmel[3], F. Montmessin[6], V. Formisano[7], M. Giuranna[7], A. Maturilli[7], T. Encrenaz[1] , [1]Observatoire de Paris, LESIA, Meudon, F-92195, France, [2]Université Pierre et Marie Curie - Paris 6, UMR 8109, Paris, F-75005, France, [3]MPS, 37191 Katlenburg-Lindau, Germany, [4]Space Research Institute (IKI), Moscow, Russia, [5]Institut Pierre Simon Laplace, LMD, Paris, F-75005, France, [6]Institut Pierre Simon Laplace, SA, Verrières-le-Buisson, F-91371, France, [6]IFSI-INAF, Roma, Italy

Introduction: Along with the cycles of pressure and dust, the water cycle is a key element of the Martian climate, involving interactions between atmospheric reservoirs and surface reservoirs. Since its initial discovery from the ground at 0.82 μm [1], Martian water vapor has been the subject of numerous telescopic observations at visible, near-infrared, thermal infrared, and millimeter/submillimeter wavelengths. In general, however, Earth-based observations have not been systematic enough to provide a global view of the seasonal cycle of water, and the climatology of Mars' atmospheric water is primarily based on spacecraft-borne measurements. The first spatially and temporally complete picture of the seasonal behavior of water was established from Viking/MAWD observations of H_2O at 1.38 μm from June 1976 through April 1979 [2]. The Viking/MAWD results, which evidenced, in particular, the Northern Polar Cap as the primary source of atmospheric water and a strong North-South asymetry in the abundance of water, remained the prime observational reference until the operation of MGS/TES in 1999-2004 [3,4]. The strengths of the MGS/TES water database include (i) its completeness over more than 2 Martian years (ii) its ability to provide simultaneous measurements of the thermal profile, dust loading, and water ice optical depth (iii) the insensitivity of the water vapor measurements to the amount of atmospheric dust. For these reasons, the TES results on the water cycle have become the usual standard on which modern Martian water climatology is based.

The water cycle was also a prime objective of the Mars Express mission, with three instruments able to measure the atmospheric water vapor content, either in the solar reflected or in the thermal component. The infrared mapping spectrometer OMEGA provides maps of water from the 2.56 μm band with high spatial and low spectral resolution. The infrared spectrometer SPICAM measures water in the 1.38 μm band with a 3.5 cm^{-1} spectral resolution [6]. Finally, the PFS instrument, which consists of two channels (long-wavelength and short-wavelength) covering altogether the 1.2-40 μm range, potentially provides measurements of water vapor both in its rotational lines (similar to TES), and in its 2.56 and 1.38 μm bands, and giving redundancy with OMEGA and SPICAM. Besides the complementarity of its instrumentation, one advantage of Mars Express with respect to the problem of the water cycle is its quasi-polar orbit, allowing in particular a detailed view of the polar caps at the sublimation onset, as already exploited by OMEGA [5]. We here report on results obtained on the long-wavelength channel of PFS.

Instrument, observation, analysis: The Planetary Fourier Spectrometer is an infrared double-pendulum interferometer working in two different channels. The short wavelength channel (SWC) covers wavenumbers from 1700 to 8200 cm^{-1} while the long wavelength channel (LWC) operates in the range 250—1700 cm^{-1}. In the present analysis we have used data from LWC only. It is characterized by an unapodized spectral resolution of 1.3 cm^{-1}, and a field of view of 50 mrad (FWHM). This corresponds to 12 kilometers on Mars surface when viewed from periapsis. A more detailed description of the PFS instrument can be found in [7]. The PFS LW channel calibration has been presented in details by [8].

Mars Express orbiter was successfully inserted into Martian orbit on December 25th, 2003, Ls=322°. The Mars Express orbiter is not located in a sun-synchronous orbit. For this reason, various local times (LT) have been covered during the mission, ranging from 8 am to 8 pm. PFS observations do not take place on each orbit, as the power and telemetry resources of the spacecraft do not allow the whole Mars Express payload to operate simultaneously. For this reason our seasonal coverage is far from complete. We here present data covering the January 2004 – December 2005 period, encompassing roughly a Martian year,

The first step in our analysis is the inversion the temperature profile as a function of pressure, which is based on the fitting of the ν_2 band of CO_2 centered at 667 cm^{-1}. Then the water rotational lines in the 250—500 cm^{-1} range is used to retrieve the Martian H_2O vapor column density. The forward radiative transfer modelling is carried out using a line-by-line model including the gaseous absorptions by CO_2 and H_2O only. The spectroscopic parameters come from the GEISA data base, except for the CO_2-broadening parameters. For water, we use the parameters

calculated by [9]. The Martian surface pressure varies strongly as a function of four parameters: season, latitude, longitude and local time. Surface pressure is predicted by interpolating the Viking Lander 1 record vertically using the accurate MOLA topography and horizontally using the meteorological pressure gradients simulated by the LMD Mars General Circulation Model [10].

The inversion of the temperature profile follows the specific algorithm designed for the inversion of the TES observations [11]. For a single PFS spectrum, the temperature is retrieved between the surface and the 10-Pa pressure level, with an uncertainty of 2 K. For the water column density retrieval, the best-fit model is estimated through the usual χ^2 cost function across the 305-505 cm^{-1} interval. The retrieved parameters are the water column density, and the surface emissivity at the different wavenumbers chosen in-between the main H_2O signatures. With the exception of the Northern Polar maximum, we estimate that the quadratic combination of various errors leads to an uncertainty of the H_2O column abundance of 2-3 pr-µm. The largest, systematic, source of uncertainty lies in the value for the CO_2-broadening parameter. The effect of increasing the CO_2-broadening parameter is to first order a linear decrease in the H_2O column abundance. Given the uncertainties on the measured parameters this gives a 25% systematic error on the retrieved water column abundance. In particular, our linewidths are about 15% larger than assumed by [3,4] in his retrieval of the water column density from the TES observations. For this reason, we retrieve a column density systematically 15% smaller than would have been retrieved by following [3] approach.

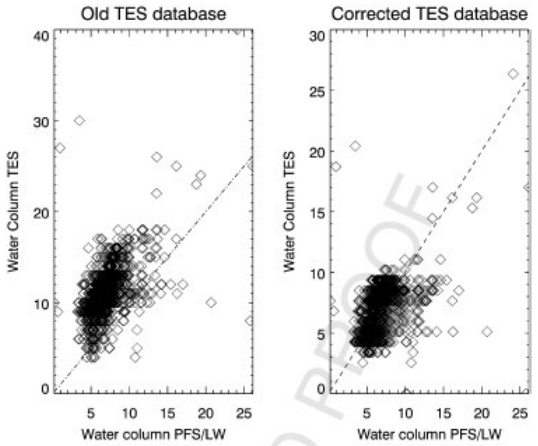

Figure. 1. Comparison of water columns retrieved from PFS/LW and TES for measurements in common epoch. Left panel: original TES retrievals. Right panel:corrected TES retrievals, using the new version of the TES database (M. Smith, priv. commun.), and a further downward 15% correction (see text for details).

Results: The seasonal distribution of the water vapor column density present some of the familiar trends of the water cycle. While the water seasonal variation inferred from PFS/LW is qualitatively similar to findings from previous space missions, our results point to a subtantially drier water cycle. In particular, the water amounts measured during the Northern summer never exceed 60 pr-µm. This contrasts to the peak column of 100 pr-µm reported by MGS/TES over the North Pole at L_s = 110°-120° for three consecutive Martian years (MY 24-26). The discrepancies between PFS/LW and TES are particularly significant since the two instruments utilize the same water features. One might, in principle, attribute them to actual temporal variability. However, TES performed systematic atmospheric measurements until 31 August 2004, providing water vapor measurements concomitant with Mars Express. These measurements were kindly provided to us by M. Smith. Figure 1 compares the water columns retrieved from PFS/LW and TES for all the points (L_s, lat) common to the two databases. It clearly indicates that the TES values are typically 1.5 times larger than the PFS/LW values. We suggest here that the TES water columns are biased towards high values. A careful re-examination of the TES retrievals by M. Smith (priv. comm., and to be published elsewhere) gives credit to this hypothesis. In brief, in Smith's reanalysis, the abundance inferred from TES is lower by about 30% than in [3,4], and a better repeatability between the three Martian years is achieved.

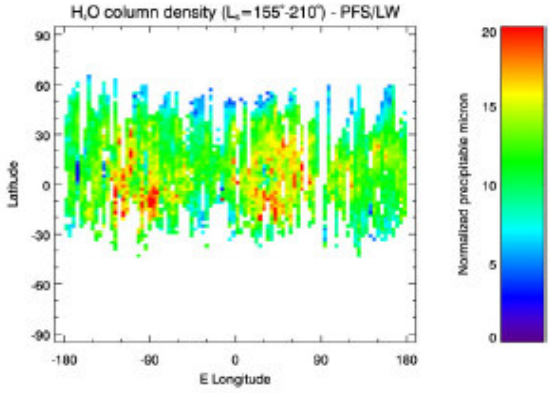

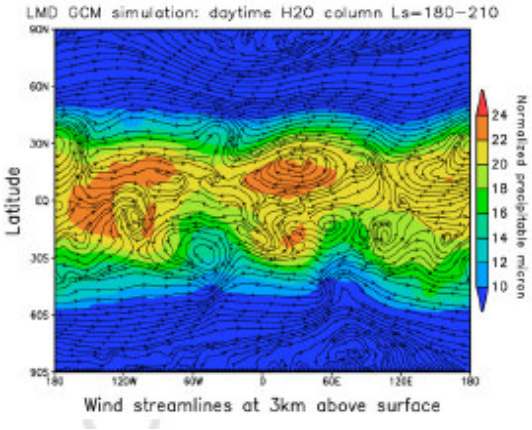

Figure 2:Top: Geographical distribution of water. Water columns are here normalized to a common 610 Pa pressure.. Bottom:: map of water vapor columns (normalized to the 610 Pa level) predicted by the LMD Global Climate Model, superimposed streamlines illustrating the mean atmospheric transport at 3 km above the surface.

Figure 2 shows water column maps as a function of latitude and longitude A weak local maxima can be distinguished at 0°-60°E and 60°-140° W in the inter-tropical region, although they appear subdued in comparison with the high-latitude maximum. These maxima, which correspond to the regions of Arabia and Tharsis, were also clearly seen in the TES data. To help interpret our water vapor observations, we performed some comparisons with the LMD/GCM, which is able to simulate the atmospheric water cycle [12]. Figure 2 shows a water column map predicted by the GCM for the season L_s=180°-210°. The simulation produces spatial variations with maxima of water vapor near Tharsis (120° W) and Arabia Terra (30° E) in qualitative agreement with the observations. This suggests that these spatial variations are probably caused by some atmospheric dynamical or physical processes, and that a subsurface water source (not included in the model) is not necessarily involved.

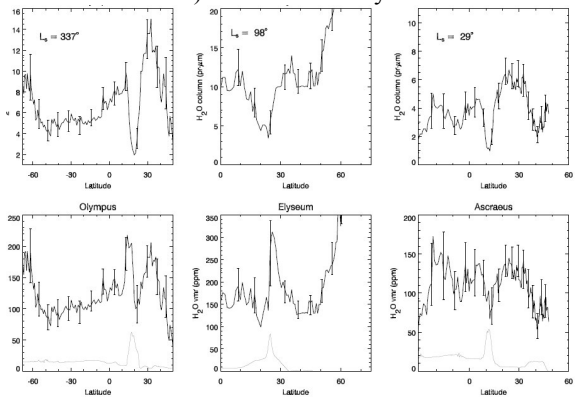

Figure 3. Absolute water columns and water volume mixing ratios below the saturation level (in part per million) in the region of three large volcanos. Olympus Mons (orbit 37), Elyseum Mons (orbit 925) and Ascraeus Mons (orbit 370). The thin lines represent the topography (arbitrary scale).

In Fig.3, we show water retrievals for three orbits crossing areas of large topographic contrast (Olympus, Elyseum, and Ascraeus). The topographic signature of the large volcanos is well visible on the absolute (unscaled) water columns. The behavior of the water volume mixing ratio below the saturation level is somewhat less clear. As shown in the bottom panels, although error bars are large, there is a suggestion for a increase of the water mixing ratio in the Southern flank of Olympus Mons, while on Elyseum results are consistent with an increase on the Northern flank. On Ascraeus Mons, there is evidence for a comparable decrease of the water abundance over the top of the volcano.. Overall, our results do not give a consistent picture for the various volcanos but indicate, at most, moderate variations of the water mixing ratio in the vicinity of the large volcanos. This result contradicts previous findings from Phobos-2/ISM observations, which indicated a factor-of-five increase in water above the volcanos and was interpreted as due to atmosphere-regolith exchanges with intense day time desorption

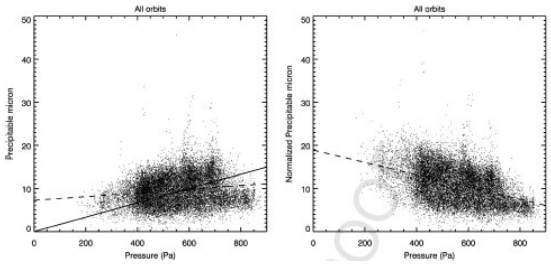

Figure 4: Absolute (left panels) and normalized to 610 Pa (right panels) water columns vs surface pressure. Dashed lines indicate best fits in the form $H2O = a + b \times P_{surf}$. The solid line in the left panels show the best fits obtained by assuming proportionality of the water columns to pressure.

Figure 4 presents the water columns (absolute and normalized to 610 Pa) as a function of pressure for the individual retrievals. To avoid large seasonal effects, and in particular the high water contents characteristic of Northern summer at high latitudes, we consider here only measurements at latitudes between 30°S and 30°N, most of which indicate water columns in the range 4-18 pr-μm. In addition, only measurements with relative uncertainties of less than 20% are included. Figure 4 indicates that, as expected for a generally well-mixed water distribution, the absolute water columns are positively correlated with pressure. However, the absolute water columns increase more slowly than they would for a linear dependence, so that the normalized water appears to be anticorrelated with

pressure. We assess the statistical significance of this result, by calculating the Spearman (rank order) correlation coefficient, and the number of standard deviations at whichthe sum-squared difference of ranks deviates from its null hypothesis expected value. This situation points to a situation intermediate between full mixing and confinement of water in a surface layer. Our results on the correlation of water with surface pressure tend to agree with those from TES. [3] reported that a linear rescaling of the water column to a fixed pressure is a slight overcompensation for topography. We have further explored whether this anti-correlation is simulated by the LMD/GCM. We found no correlation with surface pressure. This fundamental difference suggests that a key process controlling the water vapor distribution is missed by the model. In particular, the model takes into account the dynamical and saturation processes that could lead to a dependence of the water mixing ratio or the saturation altitude with the surface properties, but it does not include a subsurface source. Moreover, the observed anti-correlation between scaled water and surface pressure points to the fact that a small amount of *background* water (typically 3—4 pr-μm), may be present independently of altitude, presumably due to regolith-atmosphere exchanges.

References: Use the brief numbered style common in many abstracts, e.g., [1], [2], etc. References should then appear in numerical order in the reference list, and should use the following abbreviated style:
[1] Spinrad, H. et al.. (1963). *AJ. 137*, 1319. [2]°Farmer, C.B. et al. (1977). *JGR. 82*, 4225. [3]° Smith, M.D. (2002). *JGR 107*. 5115. [4] Smith, M.D. (2004). *Icarus 167*, 148. [6]° Fedorova, A. et al. (2006). *JGR 111*. [7] Formisano, V. et al. (2005). *PSS. 53*, 963. [8]° Giuranna, M. et al. (2005). *PSS 53*, 993. [9]°Gamache, R.R. et al. (1995). *JMS. 170*, 131. [10]° Forget, F. et al. (1999). *JGR. 104*, 24155. [11] Conrath, B.J et al (2000). *JGR 105*, 9509.